RESEARCH ARTICLE

Insights into eruption dynamics from textural analysis: the case of the May, 2008, Chaitén eruption

Fabrizio Alfano · Costanza Bonadonna · Lucia Gurioli

Abstract The May, 2008, Chaitén (southern Chile) eruption was characterized by several explosive events, each associated with plumes which reached up to about 19 km above sea level on May 6. A study of the textural and physical features of the juvenile clasts erupted during the climactic phase of the 2008 eruption of Chaitén is presented. Pumice clasts show unimodal density distribution (main mode at 600 kg/m^3), average vesicularity of about 69 %, a glassy groundmass with no microcrystals, and vesicles with dimension between ~1 μm and ~2 mm. They also show a unimodal vesicle size distribution with most frequent vesicle size in the range 0.05–0.08 mm and an estimated vesicle number density of $1.3\pm0.5\times10^5\,\mathrm{mm}^{-3}$ related to a rapid nucleation event produced during the late phases of magma rise. This is confirmed by the absence of microcrystals that

could otherwise have delayed vesicle formation and allowed the magma to maintain a low viscosity and a supersaturation in volatiles. Vesiculation and fragmentation were triggered by a sudden decompression of the melt associated with the opening of the volcanic conduit (~10 MPas^{-1}).

Introduction

Explosive-eruption dynamics are very complex and depend on a large number of parameters, such as the characteristics of the volcanic system (e.g., geometry of the conduit), the chemical and rheological characteristics of the magma involved, and the dynamics of both magma rise and fragmentation (Verhoogen 1951; Sparks 1978). As a result, textural features (e.g., bubble size and concentration) of the products of explosive eruptions provide important insights into eruption dynamics (Cheng and Lemlich 1983; Houghton and Wilson 1989; Cashman and Mangan 1994; Klug and Cashman 1996; Sahagian and Proussevitch 1998; Blower et al. 2001, 2002; Gaonac'h et al. 2005; Toramaru 2006).

Experimental and numerical studies have shown that fragmentation in silica-rich systems occurs after a rapid decompression that leads to a non-equilibrium continuous nucleation process (Blower et al. 2001, 2002). The resulting products are characterized by a high vesicle number per unit volume. In particular, textural characteristics of rhyolitic products can be considered as representative of the magma conditions at fragmentation. The content of vesicles, expressed as vesicle number density (N_V, number of vesicles per unit volume) is controlled by magma properties, such as composition, temperature, viscosity, diffusivity, and interfacial energy, and it strongly depends on the decompression rate (Toramaru 2006).

Editorial responsibility: J.E. Gardner

Electronic supplementary material The online version of this article (doi:10.1007/s00445-012-0648-3) contains supplementary material, which is available to authorized users.

F. Alfano (✉) · C. Bonadonna
Département de Minéralogie, Section des Sciences de la Terre et de L'Environnement, Université de Genève,
13, rue des Maraîchers,
CH-1205 Genève, Switzerland
e-mail: fabrizio.alfano@asu.edu

L. Gurioli
Université Blaise Pascal, Laboratoire Magmas et Volcans,
Clermont Université,
BP 10448, 63000 Clermont Ferrand, France

L. Gurioli
CNRS, UMR 6524, LMV,
63038 Clermont-Ferrand, France

L. Gurioli
IRD, R 163, LMV,
63038 Clermont-Ferrand, France

In this work, we present a detailed textural analysis of pumices lapilli produced by the May 6, 2008, Chaitén climactic phase (Layer β, 6 May; Alfano et al. 2011) with the main objective of determining the associated explosive dynamics.

The May 2008 Chaitén eruption

The May 2008 Chaitén eruption (Fig. 1a) developed from an initial highly explosive phase, which lasted approximately 2 weeks, to a second, less explosive phase characterized by dome extrusion, explosions and collapses, and the generation of pyroclastic density currents (Alfano et al. 2011). The few seismic data available indicate that the eruption was preceded by a very short period of precursory seismic signals (2 days; Lara 2009) followed by a series of several explosive events with different intensity and duration. During the initial phase, the eruptive products were dispersed to the east, over a wide area up to 600 km away from the vent, producing a tephra deposit of about 0.5 km³ bulk volume. The explosive phase reached a climax on May 6 with an associated 19-km-high column and a bulk volume of about 0.1–0.2 km³ dispersed towards the NE (Fig. 1b; Alfano et al. 2011). The pyroclastic products erupted during the climactic phase produced a lapilli-rich layer (Layer β; Alfano et al. 2011) characterized by a thickness exceeding 20 cm within 10 km from the vent (Fig. 1c). The material erupted during this phase is composed mainly of lithic fragments (~80 wt. %) produced by the disruption of the old dome, and a minor fraction of juvenile fragments represented by vesicular pumices (~10 wt.%) and fresh and not-altered obsidian fragments (~10 wt.%) (Alfano et al. 2011). The climax of the eruption was followed by a second phase started with the beginning of the dome extrusion. The shifting of activity from explosive to effusive occurred within the same explosive phase, as shown by effusion of an obsidian flow simultaneous with the explosive events are reported (Castro et al. 2012).

Fig. 1 **a** Location of the Chaitèn volcano, Chile. **b** Isopach map of the tephra fallout produced from the May 6, 2008, climactic explosion (in centimeters; modified after Alfano et al. 2011). The pumice clasts analyzed were collected about 5 km from the vent along the dispersal axis (*black circle* in figure). **c** Picture of the deposit where the clasts were collected (courtesy of Laura J. Connor, University of South Florida, USA). The deposit in this location consists, from *bottom to top*, of a basal layer of brownish ash with lithic lapilli at the very base produced by the opening explosive event of May 1–2, 2008, (*Layer α*); the lapilli layer produced during the climactic explosion of May 6, 2008 (*Layer β*); the complex sequence of tephra layers ranging from fine ash to lapilli which represents the activity after May 6, 2008, (*layers χ–ν*); a reworked layer of ash covers the entire sequence (Alfano et al. 2011). **d** Picture showing a selection of the pumice lapilli studied in this work
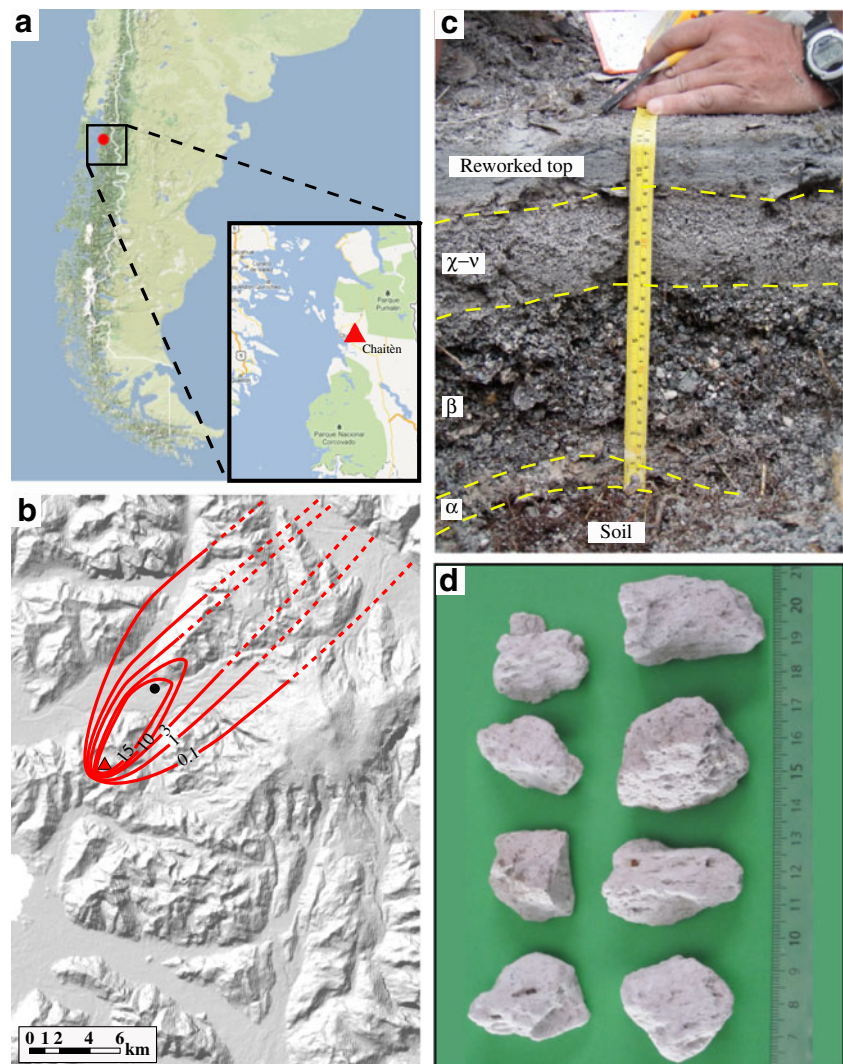
The pumices (Fig. 1d) are aphiric (<1 vol% crystals) and rhyolitic (Castro and Dingwell 2009; Alfano et al. 2011). The crystal population is composed by microphenocrysts (0.5–1.0 mm) of plagioclase, Fe-Ti oxides, orthopyroxene, and biotite, with associated rare microlites of plagioclase and biotite. The volatile fraction, mainly water, is estimated to be in the range 1.3–2.3 wt.% (Castro and Dingwell 2009). In contrast, obsidian fragments show higher degrees of crystallinity (~2–5 vol% crystals) with plagioclase crystals up to 2–3 mm diameter and a lower water content in the range 0.5–1 wt.% (Castro and Dingwell 2009). Analysis of the microlite composition and decompression experiments carried out by Castro and Dingwell (2009) have shown that the dynamics of the eruption are characterized by a rapid rise of a water-saturated rhyolitic magma from from depths of >5 km, with an estimated average velocity of about 0.5 m/s and a short magma ascent time. However, the viscosity ($\sim 10^6$–10^8 Pa s) is estimated to be at least one order of magnitude too low to produce a magma autobrecciation as a result of shear during its rise in the conduit (Castro and Dingwell 2009).

Methods

Density and porosity measurements

A density and porosity study was carried out on a population of 100 pumice lapilli (P1 to P100) of the climactic phase (i.e., Layer β, May 6; Alfano et al. 2011) collected about 5–6 km north-east of the crater. Pumice clasts are all 2–6 cm diameter (Fig. 1d) small enough, 8.5±4.9 cm³, to have cooled rapidly with little post-fragmentation vesicle expansion (Thomas and Sparks 1992; Tait et al. 1998).

The density distribution of the pumice clasts was determined using a hydrostatic balance. In order to include all the superficial vesicles in the measurement, the clasts were wrapped using parafilm (Houghton and Wilson 1989). Results were converted into bulk porosity (ratio between the volume of all the vesicles and the volume of the pumice including the vesicles) based on the average solid density measured on powdered pumice clasts using a helium pycnometer at the University of Geneva (Quantachrome ULTRAPYC 1200e). Then, 50 clasts were selected, taking care to cover the entire range of density, and a characterization of the porosity was carried out. Density measurements using the helium pycnometer were carried out on unwrapped clasts and converted using the average solid density of the powder in order to obtain the value of the closed porosity (ratio between the volume of the vesicles not connected with the surface and the volume of the pumice clasts including all the vesicles). Open porosity (ratio between the volume of the vesicles connected with the surface and the volume of the pumice clasts including

all the vesicles) was obtained by the difference between bulk and closed porosity and represents all the interconnected vesicles also connected with the surface. Relative values of open and closed porosity were also calculated as ratios between the volume of open and closed vesicles and the total volume of vesicle in each clast.

In addition, density measurements on ten juvenile obsidian clasts coeval with the pumice clasts were carried out using the helium pycnometer and represent a non-vesicular endmember of the products of the explosive event.

Textural analysis of pumice lapilli

Textures were studied of seven pumice lapilli selected from representative density classes of the pumice population (i.e., most frequent and endmember density classes; Table 1). Thin sections cut at random orientations were made from four samples, and two oriented thin sections, orthogonal and parallel to vesicle elongation, were taken from three samples (in order to represent oriented structures present in the pumice clasts). For each of the ten thin sections, a set of 17 images was acquired at four different magnifications. An image of the entire thin section was taken using a Nikon Super Coolscan 4000 (resolution 157.5 pixels/mm). Fourteen scanning electron microscope (SEM) backscatter images of parts of the thin section were taken using the JEOL JSM7001F at the University of Geneva (resolutions 267, 1,070, and 2,670 pixels/mm) following the nesting strategy described by Shea et al. (2010b). Two additional images (resolution 1,000×1,000 pixels) were extracted from the section image in order to analyze vesicles down to 0.5 mm equivalent diameter to cover the entire range of vesicle size. Images were prepared for analysis using Adobe Photoshop CS3, rebuilding manually vesicle walls and producing binary images that were processed using JMicrovision (www.jmicrovision.com). The image analysis was carried out in order to study the morphology of the vesicles, the vesicle wall thickness, and the 2D vesicle size distribution (VSD).

Vesicle morphology was studied based on the frequency distribution of the aspect ratio (AR; ratio between width and length of a vesicle) and the solidity factor (SF; ratio between the area of a vesicle and the area of the convex hull of the vesicle, which is the line of shortest distance which connects the maximum projections on a particle outline). Aspect ratio describes the elongation of the vesicle, varying between extremely elongate (<0.2), very elongate (0.2–0.4), moderately elongate (0.4–0.6), slightly elongate (0.6–0.8), and not elongate (0.8–1.0) (Blott and Pye 2008). The solidity factor describes the roughness of the outline of the vesicle. Smooth vesicles have a convex outline, with few or no concavities, so the projected area of the particle will be almost equal to the area of the convex hull and the resulting SF will be close

Table 1 Summary of data for clast density, vesicularity, and textural features for low (italic) and high (bold) density samples

Section	ρ^a	ω^b	Md Vw[c]	Md AR[d]	Md SF[e]	N_A[f]	N_V[g]	N_V[corr,h]	VSF[i]	VVF[j]	E_1[k]	E_2[l]
P48	*441*	*80*	*4.9*	*0.56*	*0.91*	*11.0*	*7.2*	*9.1*	*0.68*	*0.63*	*1.0*	*3.7*
P02$_o$	*582*	*74*	*8.0*	*0.56*	*0.91*	*7.8*	*5.5*	*6.4*	*0.53*	*0.63*	*1.2*	*3.5*
P02$_p$	*582*	*74*	*7.5*	*0.51*	*0.90*	*11.1*	*8.8*	*10.9*	*0.54*	*0.60*	*1.4*	*3.5*
P70	*670*	*70*	*6.0*	*0.46*	*0.87*	*20.2*	*16.7*	*23.4*	*0.59*	*0.50*	*1.5*	*4.2*
P38	*671*	*70*	*4.5*	*0.41*	*0.89*	*14.2*	*11.5*	*15.3*	*0.54*	*0.53*	*1.5*	*3.9*
P25$_o$	**859**	**62**	**14.8**	**0.58**	**0.86**	**9.8**	**7.9**	**12.5**	**0.38**	**0.39**	**1.5**	**3.6**
P25$_p$	**859**	**62**	**13.8**	**0.49**	**0.88**	**7.6**	**5.5**	**7.8**	**0.35**	**0.44**	**1.3**	**3.6**
P39$_o$	**1,062**	**53**	**12.0**	**0.56**	**0.87**	**12.0**	**10.1**	**13.9**	**0.39**	**0.38**	**1.5**	**4.0**
P39$_p$	**1,062**	**53**	**12.6**	**0.54**	**0.88**	**12.1**	**10.2**	**14.5**	**0.39**	**0.37**	**1.6**	**3.8**
P26	**1,271**	**43**	**10.1**	**0.49**	**0.90**	**11.0**	**9.7**	**13.1**	**0.41**	**0.32**	**1.7**	**4.0**

Values of clasts P02, P25, and P39 are reported for the orthogonal (*o*) and parallel (*p*) sections and for the average

[a] Pumice density (kilograms per cubic meters)

[b] Pumice porosity (percent)

[c] Median thickness of vesicle walls (micrometers)

[d] Median aspect ratio of the vesicles

[e] Median solidity factor of the vesicles

[f] Number vesicles per unit area (square millimeters $\times 10^2$)

[g] Number vesicles per unit volume obtained converting N_A values (cubic millimeters $\times 10^4$)

[h] Number vesicles per unit volume corrected for the vesicularity (cubic millimeters $\times 10^4$)

[i] Volume fraction of the vesicle surface area measured on thin section

[j] Volume fraction of the vesicle volume calculated from N_V values

[k] Power-law exponents of the cumulative N_V distributions trends

to 1. As roughness increases, the outline will be characterized by a larger number of concavities, and the associated SF will be reduced (Blott and Pye 2008).

Vesicle wall thickness was measured superimposing four grids of parallel lines oriented in four different directions (0°, 45°, 90°, and 135°) to the thin section images at high magnification (2,670 pixels/mm). The distribution was obtained by deleting the areas occupied by vesicles from the grid and measuring the length of the remaining segments.

VSD was studied based on the determination of the vesicle number per unit area (N_A, mm^{-2}) for each thin section and a geometric size class distribution with constant ratio $10^{-0.1}$ (Sahagian and Proussevitch 1998; Shea et al. 2010b). N_A distributions were calculated for each of the 17 images of each section, and a total N_A distribution was determined by convolution of the data obtained from each single image. N_A distributions were converted to number of vesicles per unit volume (N_V, mm^{-3}) by dividing N_A for the central value of diameter of each size class (Cheng and Lemlich 1983). The vesicle volume fraction of the sample was calculated by multiplying N_V for each bin class with the volume of the corresponding equivalent sphere. Resulting values were corrected for glass content using factor equal to the ratio between the measured and calculated porosity.

Results

Density of pumice lapilli

Pumice lapilli show a unimodal density distribution (400–1,300 kg/m^3; main mode at 700 kg/m^3; Fig. 2a) with a high-density tail, ranging between 1,000 and 1,300 kg/m^3 (i.e., ~10 % of the distribution; Fig. 2a). Bulk porosity, calculated based on helium pycnometer bulk density of 2,242±14 kg/m^3, ranges between 43 % and 80 %. No clear correlation between pumice volume and porosity was found. Porosity analyses were carried out on 38 pumice lapilli with densities less than 800 kg/m^3, representing the most frequent density classes, and on 12 pumice clasts from the high-density tail. Bulk and open porosity decrease accordingly, with an average value of the open porosity equal to 53±9 %. In contrast, closed porosity remains roughly constant, with an average value of 15±4 % (Fig. 2b). Relative open porosity varies between 70 % and 86 % of the bulk porosity. In contrast, closed porosity varies between 14 % and 30 % of the bulk porosity showing a slightly increase for the high-density tail pumice clasts (27± 11 %) with respect to the pumice clasts with density less than 800 kg/m^3 (21±5 %) (Fig. 2b).

Obsidian lapilli are characterized by helium pycnometer density of 2,267±33 kg/m^3, very close to solids density of
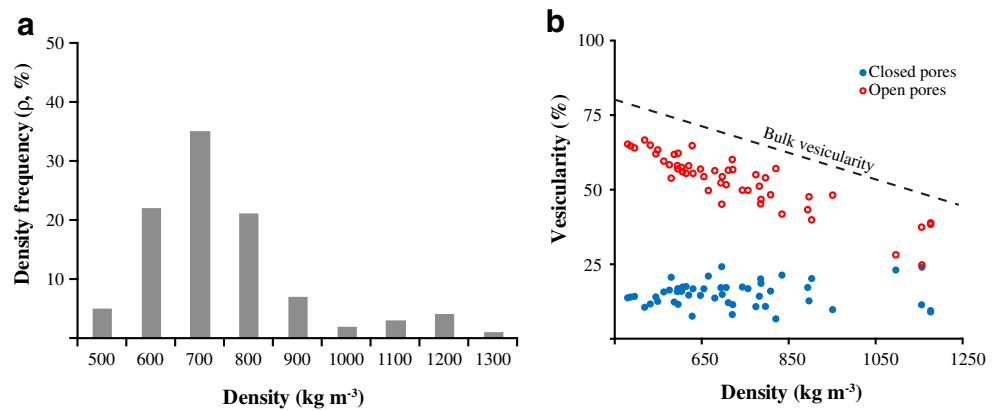
the powdered pumice clasts (2,242±14 kg/m³), which indicates that these products can be considered as not vesicular.

Description of the thin sections

A qualitative and quantitative characterization of the vesicles was carried out on pumice lapilli of both endmembers and modal density classes (Fig. 2a). Analyses on sections with generic orientation have been carried out on samples P48, P70, P38, and P26; analyses on orientated sections have been carried out on samples P02, P25, and P39.

The analyzed pumice lapilli are characterized by highly stretched vesicles and an almost crystal-free glass groundmass (Fig. 3a). No evidence of post-fragmentation expansion or breadcrusting was observed. Vesicles tend to be larger in clasts with lower density, and coalescence is greater in low-density clasts (cf., P48, P02, P70, and P38, Fig. 3a). Vesicle morphologies are highly irregular, and no particular differences are observed in sections oriented perpendicular and parallel to vesicle elongation (cf., P02, P25, and P39, Fig. 3a). Vesicles in low-density clasts show regular shapes with regular convex outlines (cf., P02, P25, and P39, Fig. 3a). High-density pumice clasts are characterized by stretched vesicles occasionally presenting indented walls (cf., P25 and P39, Fig. 3a). Aspect ratios show unimodal distribution for all the analyzed sections except for the P25 parallel section (Fig. 3b). Vesicles generally show a high degree of elongation, with median values of AR ranging between 0.4 and 0.6. A slightly higher degree of elongation is found for samples P70 and P38 (cf., Table 1). Sections orthogonal to the direction of vesicle elongation show AR values slightly higher than sections parallel to it (difference <10 %). Vesicles have various shapes, with SF varying widely from 0.3 to 1. Outlines of vesicles are more irregular for the most elongate vesicles, with SF (Table 1) varying from high values (about 0.9=regular outline), for slightly and not elongate vesicles, and decreasing progressively as elongation increases. This behavior is particularly evident in

samples P25 and P39, where vesicles with high elongation can be very irregular (SF<0.7).

In order to investigate the distribution of vesicle walls, samples were divided in two groups by density: low-density samples (blue symbols; P48, P02, P38, and P70; density between 441 and 671 kg/m³) and high-density samples (red symbols; P25, P39, and P26; density between 859 and 1,271 kg/m³) (Fig. 3b). Median thickness of vesicle walls are in the range 4–8 and 10–15 μm for low- and high-density samples, respectively (Fig. 4), corresponding to a 2D glass fraction of 0.3–0.5 and 0.6–0.7.

Vesicle size distribution (VSD)

Despite vesicles being texturally different in terms of their morphology and wall thickness, only slight variations in the VSD are observed. N_A is similar for all samples, equal to $1.3 \pm 0.5 \times 10^3 \, mm^{-2}$ for the low-density samples to $1.0 \pm 0.2 \times 10^3 \, mm^{-2}$ for the high-density samples. Average vesicle number per unit area is $1.2 \pm 0.4 \times 10^3 \, mm^{-2}$. As a result, N_V gives similar values for the two density classes of samples ($9.9 \pm 4.4 \times 10^4 \, mm^{-3}$ for low-density pumice clasts and to $8.7 \pm 2.0 \times 10^4 \, mm^{-3}$ for high-density pumice clasts). These values correspond to different ranges of vesicle volume fraction (VVF) equal to 0.50–0.63 and 0.32–0.44 for low- and high-density pumice clasts, respectively (cf., Table 1).

Distribution of vesicle sizes are described plotting volume fractions (corrected for the melt) with vesicle sizes expressed as diameters of equivalent spheres (Fig. 5). Vesicle size are distributed unimodally with mode of 0.05–0.08 mm, with the only exception of the orthogonal section of P02 and the parallel section of P25 that show mode at 0.08–0.13 mm. Observed minimum and maximum sizes of the vesicles are ~0.01 and ~3 mm, respectively. Vesicles with equivalent diameter larger than 1 mm are mostly present in the clasts with the lowest density (P48 and P02). VSD is similar for all clasts and do not vary with the orientation of the sections nor with respect to vesicle elongation.

Fig. 3 a Selection of SEM images for some analyzed clasts with increasing density from *top to bottom*. Vesicles are in *black*, glass walls in *white*. Width of the images is indicated for each magnification (millimeters). Clasts number is indicated on the *right*. b Frequency distribution of aspect ratio (AR) of the vesicles of all the low- and high-density pumice clasts analyzed in this work
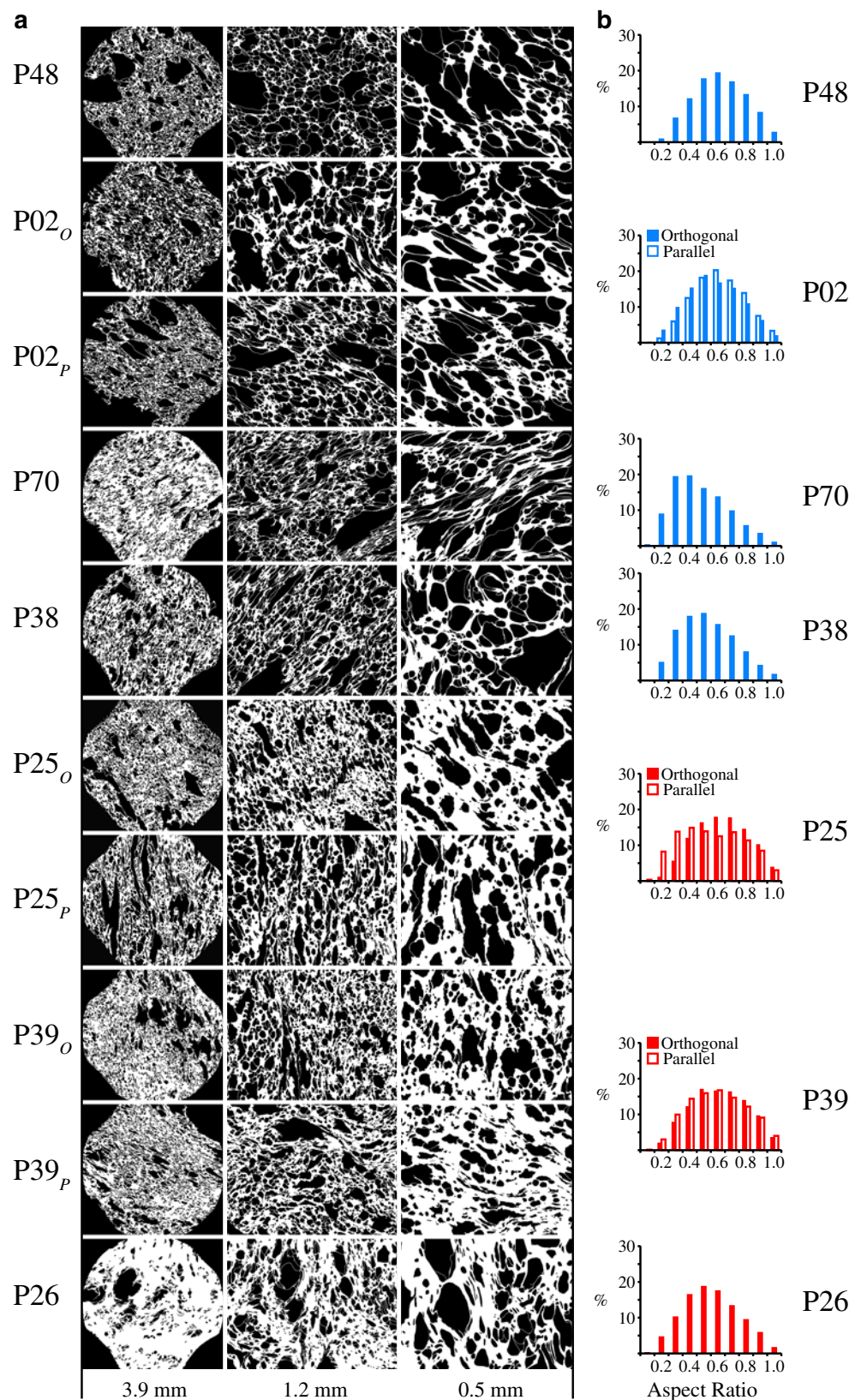
Volume fraction of the analyzed clasts was normalized to the average VSD to better compare associated textures and show similar distributions (Fig. 6a). The most significant exceptions are represented by the content in vesicles <0.03 mm for the sample P70 and the content in large vesicles (>0.3 mm) for the low-density samples (P48 and
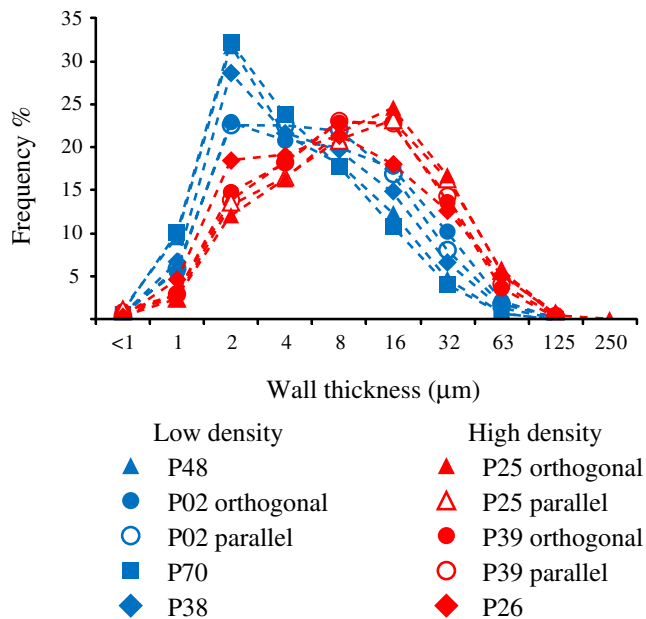
Fig. 4 Thickness distribution of vesicle walls based on the measured length of the segments connecting adjacent vesicles

P02). Nonetheless, all samples show similar values in the range 0.05–0.13 mm, in agreement with the modes of the volume fraction distributions. Given the small differences between samples, an average N_V^{corr} distribution inferred for the bulk magma was calculated, and the converted cumulative number density ($N_V^{corr} > d$; cubic millimeter) was plotted versus particle diameter (Fig. 6b). The distribution is characterized by two populations of vesicles, both of which follow power-law trends with different slope. For small vesicles ($d < 16$ μm), $N_V^{corr} > d$ is characterized by a power-law trend with exponent (E_1) equal to 1.1. For larger vesicles ($d > 16$ μm), $N_V^{corr} > d$ is characterized by a power-law trend with exponent (E_2) equal to 3.6. However, power-law exponents E_1 and E_2 for individual samples vary respectively in the ranges 1.0–1.7 and 3.5–4.2 (cf., Table 1). As a result, the average number of vesicles per unit volume corrected for the melt (N_V^{corr}) inferred for this explosive phase is $1.3 \pm 0.5 \times 10^5$ mm^{-3}.

Figure 7 shows the relation between mass eruption rate (MER, kilograms per second; Wilson and Walker 1987) and the N_V for the Chaitén explosion of May 6, 2008, and other studied eruptions of basaltic, rhyolitic, and phonolitic magmas. Basaltic eruptions seem to show a trend between MER and N_V, whereas rhyolitic and phonolitic eruptions do not. Values of the eruptive parameters of all the eruptions are collected in Table 2.

Decompression rate

The decompression rate that characterized the Chaitén climactic phase of May 6, 2008, was calculated using the

model of Toramaru (2006) defined for homogeneous nucleation of the vesicles. A rhyolitic magma (74 SiO$_2$wt.%; Alfano et al. 2011) rich in volatiles (2–5 H$_2$Owt.%) and a temperature interval in the range 775–850 °C were considered (Castro and Dingwell 2009). Only vesicles with diameter <0.01 mm (Shea et al. 2011) have been considered in the calculation, assuming they correspond to the last nucleation event before the fragmentation ($N_V^f = 7.3 \pm 3.0 \times 10^4$ mm^{-3}). The resulting decompression rate is on order of 8.1 ± 2.9 MPas^{-1}, corresponding to an exit velocity in the range 330–790 m/s (assuming a mixture composed of 50 % vesiculated magma and 50 % not-vesiculated magma with density $1,490 \pm 100$ kg/m^3). If the total N_V^{corr} is considered, the value of the estimated decompression rate increases to 12.1 ± 4.3 MPas^{-1}, corresponding to an exit velocity in the range 490–1,180 m/s.

Discussion

Pumice lapilli erupted during the climactic phase of May 6, 2008, of Chaitén volcano are characterized by a unimodal VSD with a predominance of small vesicles with modal diameter between 0.05 and 0.08 mm (Fig. 5) that does not vary significantly with clast density. Unimodal distribution and the high frequency of small vesicles suggest that vesiculation occurred over a very short time and relatively late during magma ascent (Klug et al. 2002), as also suggested by the absence of microcrystals and by the relatively low viscosity (~10^6–10^8 Pas^{-1}) of the rhyolitic melt (Castro and Dingwell 2009). Given that there was not enough time for vesicles to expand, only a small number of vesicles with diameter >1 mm was observed, and they are only present in the clasts with low density (P48 and P02; cf, Figs. 3a and 5).

The lack of large vesicles in the dense pumice clasts may be also enhanced by processes of collapse that produced the irregular vesicles characterized by lower values of SF observed in sections P25 and P39 (cf., Table 1 and Fig. 4a). Open porosity shows high values suggesting that coalescence may have played a role in the evolution of magma porosity. However, it is also possible that fractured vesicle walls might have contributed to reach these high values. Open porosity increases along with the bulk porosity, as the probability of vesicles to coalesce producing a complex network of interconnected vesicles increases with the number and the volume of the vesicles. This may have favored the degassing process that produced the collapsed vesicles observed in samples P25 and P39. Pumice lapilli of the high-density tail show how an increase in relative closed porosity corresponds to a decrease in open porosity through collapse processes.

Cumulative N_V plots produce power-law trends that are usually interpreted as the result of vesicle nucleation under non-equilibrium conditions, which is characteristic of

Fig. 5 VSD expressed in volume fraction corrected for the melt for all the low and high density pumice clasts analyzed in this study. The average vesicle volume fraction is reported for each single plot
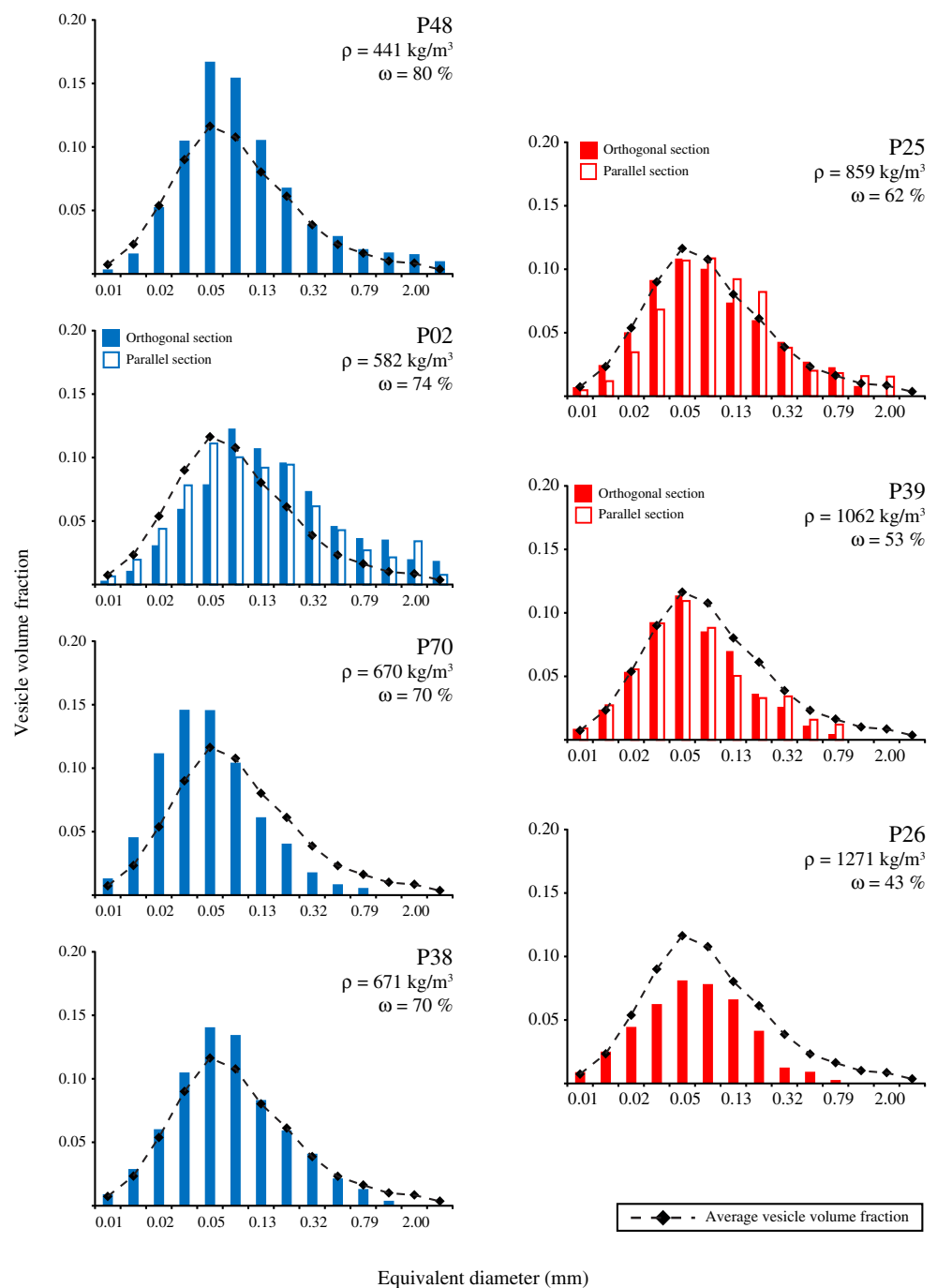
explosive eruptions, especially of silica-rich magmas (Mangan and Cashman 1996; Blower et al. 2001, 2002). In fact, similar trends are reported for the products of the 1875 eruption of Askja volcano, which show VSD characterized by two power-law trends with the branch representing intermediate and coarse vesicle size characterized by exponents in the range 2.3–5.1 (Carey et al. 2009). In addition, the 1980 Mt. St. Helens eruption shows a power-law trend with exponent of about 3.4 (Rust and Cashman 2011), and the 1912 eruption of Novarupta shows a power law-trend with exponent of 3.9 (Adams et al. 2006a, b).

The relation between the evolution of the volatile fraction present within a melt and the explosivity of the eruption is not totally understood. Considering the values of MER and N_V (cf. Table 2 and Fig. 7), Chaitén volcano's May 6 explosion is characterized by values close to those estimated for layers 2 and 5 of Cotopaxi, Etna 122 BC, and units B, D, and F of Towada volcano. Differences of at least one order of magnitude in the values of MER and N_V are observed when comparing Chaitén eruption with the other cases reported in Table 2. Houghton et al. (2010) assert that there is a positive correlation between MER and N_V. According to

Fig. 6 a VSD expressed in volume fraction normalized for the average volume fraction (volume fraction/average volume fraction) for all the analyzed samples showing the differences in vesicle populations. *Symbols* as in Fig. 5. **b** Average cumulative N_V^{corr} distribution. Standard deviation is indicated for each point
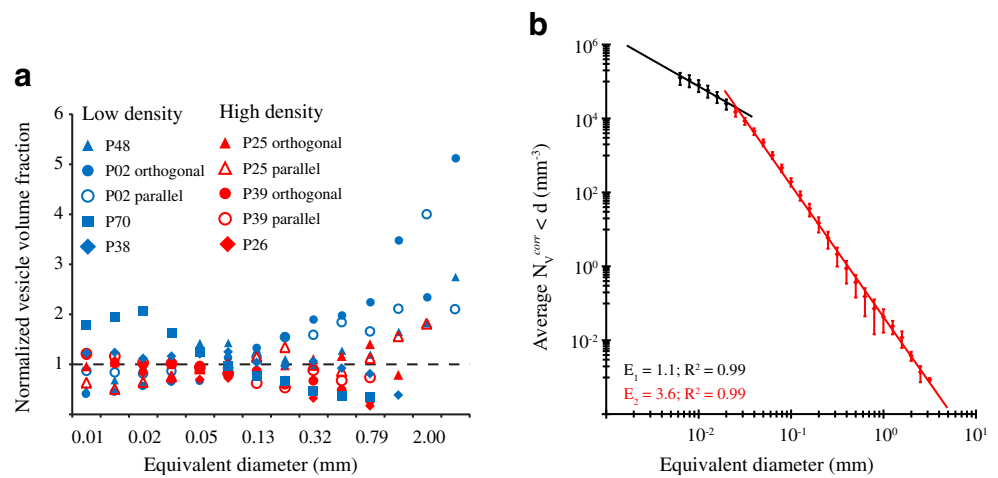
Rust and Cashman ([2011]), this correlation cannot be generalized to all cases, and it is limited to those cases in which vesiculation occurs in near-equilibrium condition. Basaltic eruptions show an increase of the vesicle number density with the mass eruption rate associated with a shift in the eruptive style from Hawaiian/Strombolian (Kilauea Iki,

Fig. 7 Log–log plot of the mass eruption rate (MER) versus the vesicle number density corrected for the melt (N_V^{corr}). References as in Table 2
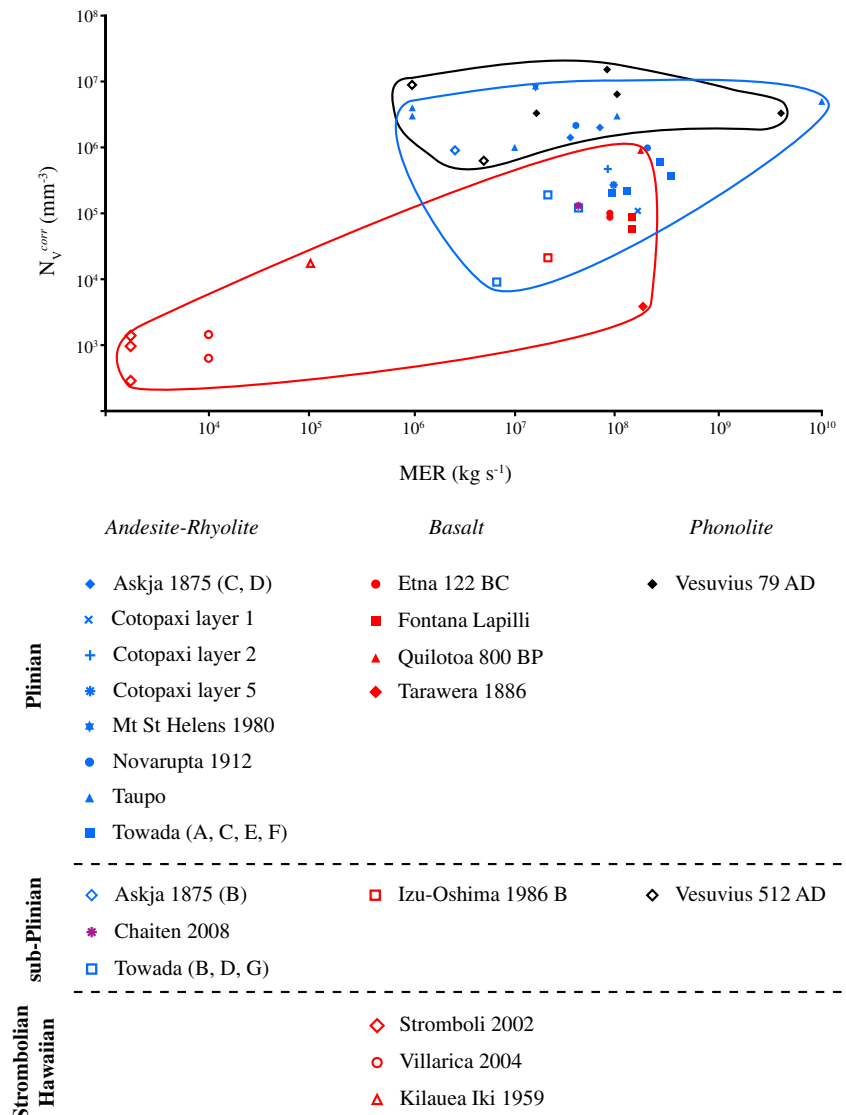
Table 2 Summary table of main eruptive parameters of studied eruptions

Eruption		Eruptive style	H_T, km	MER, kgs^{-1}	SiO$_2$, %	N_V, mm^{-3}	$\Delta P/\Delta t$, MPas^{-1}
Askja 1875	Unit B	Sub-Plinian	8	2.6×10^6	55–70	9.0×10^5	–
	Unit C	Plinian	23	6.8×10^7	55–70	2.0×10^6	–
	Unit D		26	3.5×10^7		1.4×10^6	–
Chaitén	May 6, 2008	Sub-Plinian	19	4.2×10^7	74.2	1.3×10^5	$7.9\pm2.8\times10^0$
Cotopaxi	Layer 1	Plinian	33	1.6×10^8	56.7	1.1×10^5	–
	Layer 2		28	8.1×10^7	59.1	4.8×10^5	–
	Layer 5		29	9.3×10^7	57.9	2.7×10^5	–
Etna 122 BC	Unit C	Plinian	26	8.5×10^7	49	1.0×10^5	–
	Unit E		26	8.5×10^7	49	8.7×10^4	–
Fontana lapilli							
60 ka BP	Microlite-rich	Plinian	32	1.4×10^8	53	8.7×10^4	–
	Microlite-poor					5.8×10^4	–
Izu Oshima	1986 B	Sub-Plinian	16	2.1×10^7	55.0	2.1×10^4	4.9×10^0
Kilauea Iki	1959	Hawaiian	0.6	1.0×10^5	50.0	1.8×10^4	
Mt. St. Helens	1980	Plinian	19	1.9×10^7	66.0	8.2×10^6	1.4×10^2
Novarupta 1912	Ep. II	Plinian	22–25	2.0×10^8	73–78	9.6×10^5	–
	Ep. III		17–23	4.0×10^7		2.1×10^6	–
Quilotoa 800 BP	800 BP	Plinian	35	1.7×10^8	74–78	$8.1–8.9\times10^5$	–
Stromboli 2002	18–22 May	Strombolian	0.1–0.3	2–1700	52.5	0.3×10^3	–
	30 Sep to 1 Oct		0.1–0.4			$0.4–1.1\times10^3$	–
	28 Dec		0.1–0.3			1.3×10^3	–
Tarawera	1886	Plinian	≥28	1.8×10^8	51.0	4.0×10^3	–
Taupo 1.8 ka	Unit 2	Plinian	55	1.0×10^7	74.0	1.0×10^6	–
	Unit 3			1.0×10^6		4.0×10^6	–
	Unit 4			1.0×10^6		3.0×10^5	–
	Unit 5			1.0×10^8		3.0×10^6	–
	Unit 6			1.0×10^{10}		5.0×10^6	–
Towada	A	Plinian	30	2.6×10^8	71.4	6.0×10^5	6.4×10^1
	B	Sub-Plinian	19	4.2×10^7	74.2	1.2×10^5	1.8×10^1
	C	Plinian	32	3.4×10^8	66.7	3.7×10^5	7.0×10^1
	D	Sub-Plinian	16	2.1×10^7	67.8	1.9×10^5	4.1×10^1
	E	Plinian	25	1.3×10^8	65.7	2.2×10^5	5.6×10^1
	F		23	9.0×10^7	61.1	2.0×10^5	9.1×10^1
	G	Sub-Plinian	12	6.7×10^6	66.1	9.0×10^3	6.3×10^0
Vesuvius 79 AD	EU1 fall	Plinian	15	1.6×10^7	54.1	3.30×10^6	0.4×10^0
	EU2 fall		26	8×10^7	55.4	1.52×10^7	1.1×10^0
	EU3 max		29	1×10^8	54.7	6.40×10^6	6.2×10^0
	EU4 fall		23	4×10^9	54.1	3.30×10^6	0.4×10^0
Vesuvius 512 AD	U5	Sub-Plinian	7–15	5.0×10^6	59.0	$1.4–6.3\times10^5$	–
	U7		6–9	1.0×10^6		$1.2–8.9\times10^5$	–
Villarica 2004	Scoria	Hawaiian	≥0.08	1.0×10^4	54.1	$0.4–1.6\times10^3$	–
	Golden Pumice					$0.1–0.7\times10^3$	–

Values of MER in italic characters are calculated based on the column height (Wilson and Walker 1987); values of decompression rate are calculated based on the model of Toramaru (2006)

H_T column height, *MER* mass eruption rate, *SiO$_2$* silica wt.%, $\Delta P/\Delta t$ decompression rate

References: Carey et al. (2009), (2010) [Askja 1875]; this work, Alfano et al. (2011); [Chaitén 2008]; Barberi et al. (1995); Costantini (2010); Biass and Bonadonna (2011); Pistolesi et al. (2011) [Cotopaxi]; Coltelli et al. (1998); Houghton et al. (2004); Sable et al. (2006), 2009; [Etna 122 BC]; Costantini et al. (2010) [Fontana Lapilli 60 ka BP]; Toramaru (1990); Blower et al. (2002); Toramaru (2006); [Izu Oshima 1986]; Helz (1987); Parfitt (1998); Wallace and Anderson (1998); Parfit and Wilson (1999); Stoval et al. (2011); [Kilauea Iki 1959]; Klug and Cashmann (1994); Toramaru (2006) [Mt. St. Helens]; Fierstein and Hildreth (1992); Adams et al. (2006a), b [Novarupta 1912]; Rosi et al. (2004) [Quilotoa 800 BP]; Metrich et al. (2001); Lautze and Houghton (2005); Patrick (2005); Lautze and Houghton (2007), (2008) [Stromboli 2002]; Walker et al. (1984); Sable et al. (2009); [Tarawera 1886]; Wilson and Walker (1985); Wilson (1993); Sutton et al. (1995), (2000); Houghton et al. (2010) [Taupo 1.8 ka]; Toramaru (1990); Blower et al. (2002); Toramaru (2006) [Towada]; Carey and Sigurdson (1987), Gurioli et al. (2005); Shea et al. (2010a, b), (2011) [Vesuvius 79 AD]; Cioni et al. (2011) [Vesuvius 512 AD]; Witter et al. (2004); Gurioli et al. (2008) [Villarica 2004]

1959; Stromboli, 2002; Villarica, 2004) to sub-Plinian (Izu-Oshima, 1986) and Plinian eruptions (Etna 122 BC, Fontana Lapilli and Quilotoa 800 BC, Tarawera, 1886). Vesicle number density of phonolithic eruptions does not show a clear correlation with eruption style (e.g., Vesuvius 512 AD and Vesuvius 79 AD), but more phonolitic eruptions should be studied to confirm this observation. More complex is the behavior of andesitic/ rhyolitic eruptions. Sub-Plinian andesitic/rhyolitic eruptions (Chaitén May 6, 2008, and Towada volcano Units B, D, and G) follow the trend of basaltic Plinian/sub-Plinian eruptions, with the exception of the Unit B of the 1875 Askja eruption, which shows N_V values more similar to Plinian andesitic/rhyolitic eruptions. Andesitic/ rhyolitic Plinian eruptions partially follow the trend of basaltic Plinian/sub-Plinian eruptions (Cotopaxi layers 1, 2, and 5, Novarupta episode II, and Towada Units A, C, E, and F) and partially the trend of phonolitic eruptions (Askja 1875 Units C and D, Mt. St. Helens May 18, 1980, Novarupta 1912 episode III, and Taupo 1.8 ka). It is important to notice that the MER range is similar for most Plinian/sub-Plinian eruptions independently on the composition (i.e., mostly 10^6–10^9 kg/s), while the largest N_V values are shown by both Plinian andesitic/rhyolitic eruptions and Phonolitic eruptions. The lowest MER and N_V values are shown by Strombolian and Hawaiian eruptions. We can conclude that Plinian and sub-Plinian eruptions are difficult to distinguish only based on N_V and MER values (with N_V mostly >10^4 mm^{-3} with the exception of Tarawera 1886) but are very different from Strombolian and Hawaiian eruptions that are characterized by MER<10^5 kg/s and N_V<5×10^4 mm^{-3}. Regardless of the general trends shown by Fig. 7, the relation between N_V and MER is complex, especially when we consider the high degree of uncertainty in the determination of both parameters. The high uncertainty in N_V results from determination obtained typically by the statistical 2D analysis of pumice samples, with the assumption that a small number of pumice clasts can be considered a representative of the whole magma. In addition, MER can be currently estimated only within a factor of 10 due to the large uncertainties associated with both the existing expressions that relate plume height and MER and the current strategies used to determine the erupted mass and plume height (Mastin et al. 2009).

The textural features found in Chaitén products suggest an eruption driven by a violent decompression of the magmatic system that triggered the homogeneous vesiculation of a water super-saturated magma. Considering the large content of lithic fragments (~80 %; Alfano et al. 2011), we think that this sub-Plinian event was generated by the disruption of the old obsidian dome and the consequent opening of an ~800-m radius vent (Smithsonian Institution 2008). According to the calculated N_V, for a temperature

interval of 775–850 °C and a water content of 2–5 wt.%, the decompression rate estimated to have produced such a sub-Plinian explosion is about 10 MPas^{-1} (Toramaru 2006). This value of decompression rate agrees with values calculated for past eruptions and presented by Toramaru (2006) using the decompression rate meter for homogeneous nucleation. As an example, the Chaitén explosion of May 6 shows values of column height, composition, and N_V (cf., Table 2) similar to the sub-Plinian episodes of the historical eruptions of Towada caldera and Izu-Oshima (Toramaru 1990, 2006; Blower et al. 2002), whose decompression rate is estimated to have been in the range between 6.3– 91.0 MPas^{-1}, for Towada caldera, and 4.9 MPas^{-1}, for Izu-Oshima (cf., Table 2). This behavior is related to the different mechanism controlling vesiculation. In basaltic magmas, where the viscosity is low, vesiculation is controlled by diffusion and coalescence, with the result that same decompression rates produce lower N_V than in rhyolitic melts, where vesiculation is controlled by the high viscosity (Toramaru 1995; Klug and Cashman 1996). In contrast, the values of N_V and decompression rate estimated for the 1980 eruption of Mt. St. Helens are one order of magnitude higher than those estimated for the Chaitén explosion. In this particular case, the sector-collapse that triggered the eruption (Holasek and Self 1995) caused a high decompression rate.

Crystallinity can play a role in eruption dynamics. As an example, the decompression rate values calculated for the 79 AD eruption of Vesuvius (Shea et al. 2011) assuming an heterogeneous nucleation of the vesicles gives values in the range 0.4–6.2 MPas^{-1}, in the same order as those for the Chaitén eruption. The 79 AD Plinian eruption of Vesuvius (cf., Table 2: Gurioli et al. 2005; Shea et al. 2010a) is characterized by N_V of one to two orders of magnitude higher than the N_V calculated for the pumice clasts of Chaitén. This aspect shows the important effect that the absence of microcrystals in Chaitén melt had on the eruption dynamics, as higher decompression rate are required to trigger vesiculation.

The presence of 10 % of non-vesicular, juvenile obsidian fragments within the tephra deposit and the simultaneous obsidian effusion documented by Castro et al. (2012) suggest that the pumice lapilli are the relict of a volatile-rich batch of magma, which was involved in the very beginning of the eruption. The abrupt difference in density and porosity of pumice and obsidian clasts and the lack of intermediate varieties indicate a dynamic of eruption involving volatile-rich magma and so was able to vesiculate and produce the sub-Plinian phase and a volatile-poor magma. Castro et al. (2012) explain the relation between the volatile-rich and the volatile-poor magma as the result of a degassing through a magma fracturing process induced by shear stress. The collapse morphology observed in the vesicles of the

high-density samples indicates clearly that a degassing process was developing during the magma rise. In addition, all the samples, regardless of density have highly elongated vesicles, with medium AR in the range 0.4–0.6 (cf., Fig. 3b), indicating that a high shear stress was acting on the magma body, extending its influence to the middle of the conduit, as a result of both the high ascent velocity of the magma (0.5 m/s; Castro and Dingwell 2009) and its rise through a narrow dike (Wicks et al. 2011). However, the low values of viscosity (Castro and Dingwell 2009) and the degassing process acting on the magma body (Castro et al. 2012) indicate that conditions did not favor magma autobrecciation. Consequently, there must have been other factors acting on the system that triggered of the explosive phase. Fast ascent, enhanced by the low viscosity of the magma, and the absence of microcrystals did not allow for a significant vesicle nucleation and growth, reducing the efficiency of the shear-induced degassing. As a result, large portions of the magma body could reach shallow crustal levels highly supersaturated in water. In this situation, the preexisting dome had a critical role acting as a plug obstructing the volcanic conduit and causing pressure to increase. When failure of the dome occurred, the magma decompressed rapidly, triggering the nucleation of bubbles and the consequent sub-Plinian eruption that produced the Layer β deposit.

Conclusions

- The juvenile products, in the size range 2–6 cm, of the climactic sub-Plinian explosion of May 6, 2008, of Chaitén volcano (Layer β) are characterized by a density range 400–1300 kgm^{-3} (bulk vesicularity ranging between 54 vol.% and 81 vol.%) with vesicle diameters <4 mm, irregular vesicle morphologies, some vesicle collapse structures, median vesicle walls thickness varying between 4 and 15 μm, and unimodal VSD with modal values in the range 0.05–0.08 mm and a total N_V of $1.3\pm0.5\times10^5 mm^{-3}$.
- The open porosity decreases with bulk porosity and represents the main fraction of the vesicles in the clasts (78±8 %). This high degree of interconnection between vesicles favored degassing processes that produced morphologies of vesicle collapse and a higher fraction of closed porosity observed in the pumice clasts with high density (21±5 % for pumice clasts with density >800 kgm^{-3}; 27±11 % for pumice clasts with density <800 kgm^{-3}).
- Unimodal VSD and the power-law trend of the cumulative N_V plots indicate that the magma was not in equilibrium with the volatile fraction and produced a rapid and continuous homogeneous nucleation that occurred

in the later phases of the magma rise through the conduit. The rapid rise and the absence of microcrystals delayed the magma degassing that started at shallow levels.
- Fragmentation was triggered by the nucleation of vesicles due to a sudden decrease of pressure estimated to be about 10 $MPas^{-1}$, produced by the failure of the preexisting obsidian dome during magma rise. After a highly explosive phase, the activity shifted to the effusive phase that involved volatile-poor magma, which started to erupt simultaneously with the explosive activity. Relics of this magma batch are included in the tephra deposit as non-vesicular obsidian clasts.

References

Adams NK, Houghton BF, Fagents SA, Hildreth W (2006a) The transition from explosive to effusive eruptive regime: the example of the 1912 Novarupta eruption, Alaska. Geol Soc Am Bull 118 (5–6):620–634

Adams NK, Houghton BF, Hildreth W (2006b) Abrupt transitions during sustained explosive eruptions: examples from the 1912 eruption of Novarupta, Alaska. Bull Volcanol 69(2):189–206

Alfano F, Bonadonna C, Volentik ACM, Connor CB, Watt SFL, Pyle DM, Connor LJ (2011) Tephra stratigraphy and eruptive volume of the May, 2008, Chaiten eruption, Chile. Bull Volcanol 73 (5):613–630

Barberi F, Coltelli M, Frullani A, Rosi M, Almeida E (1995) Chronology and dispersal characteristics of recently (last 5000 years) erupted tephra of Cotopaxi (Ecuador): implications for long-term eruptive forecasting. J Volcanol Geoth Res 69:217–239

Biass S, Bonadonna C (2011) A quantitative uncertainty assessment of eruptive parameters derived from tephra deposits: the example of two large eruptions of Cotopaxi volcano, Ecuador. Bull Volcanol 73(1):73–90

Blott SJ, Pye K (2008) Particle shape: a review and new methods of characterization and classification. Sedimentol 55(1):31–63

Blower JD, Keating JP, Mader HM, Phillips JC (2001) Inferring volcanic degassing processes from vesicle size distributions. Geophys Res Lett 28(2):347–350

Blower JD, Keating JP, Mader HM, Phillips JC (2002) The evolution of bubble size distributions in volcanic eruptions. J Volcanol Geoth Res 120(1–2):1–23

Carey S, Sigurdsson H (1987) Temporal variations in column height and magma discharge rate during the 79 AD eruption of Vesuvius. Geol Soc Am Bull 99(2):303–314

Carey RJ, Houghton BF, Thordarson T (2009) Abrupt shifts between wet and dry phases of the 1875 eruption of Askja volcano:

microscopic evidence for macroscopic dynamics. J Volcanol Geoth Res 184(3–4):256–270

Carey RJ, Houghton BF, Thordarson T (2010) Tephra dispersal and eruption dynamics of wet and dry phases of the 1875 eruption of Askja volcano, Iceland. Bull Volcanol 72(3):259–278

Cashman KV, Mangan MT (1994) Physical aspects of magmatic degassing .2. Constraints on vesiculation processes from textural studies of eruptive products. In: Caroll M (ed) Volatiles in magmas. Min Soc Am. pp 447–478

Castro JM, Dingwell DB (2009) Rapid ascent of rhyolitic magma at Chaiten volcano, Chile. Nat 461(7265):780–U729

Castro JM, Cordonnier B, Tuffen H, Tobin MJ, Puskar L, Martin MC, Bechtel HA (2012) The role of melt-fracture degassing in defusing explosive rhyolite eruptions at volcán Chaitén. Earth Planet Sci Lett 333–334:63–69

Cheng HC, Lemlich R (1983) Errors in the measurement of bubble-size distribution in foam. Ind Eng Chem Fund 22(1):105–109

Cioni R, Bertagnini A, Andronico D, Cole PD, Mundula F (2011) The 512 AD eruption of Vesuvius: complex dynamics of a small scale subplinian event. Bull Volcanol 73(7):789–810

Coltelli M, Del Carlo P, Vezzoli L (1998) Discovery of a Plinian basaltic eruption of Roman age at Etna volcano, Italy. Geol 26 (12):1095–1098

Costantini L (2010) Understanding basaltic explosive volcanism. In: Terre & Environnement. Université de Genève, Genève, p 166

Costantini L, Houghton BF, Bonadonna C (2010) Constraints on eruption dynamics of basaltic explosive activity derived from chemical and microtextural study: the example of the Fontana Lapilli Plinian eruption, Nicaragua. J Volcanol Geoth Res 189(3–4):207–224

Fierstein J, Hildreth W (1992) The Plinian eruptions of 1912 at Novarupta, Katmai National Park, Alaska. Bull Volcanol 54:646–684

Gaonac'h H, Lovejoy S, Schertzer D (2005) Scaling vesicle distributions and volcanic eruptions. Bull Volcanol 67(4):350–357

Gurioli L, Houghton BF, Cashman KV, Cioni R (2005) Complex changes in eruption dynamics during the 79 AD eruption of Vesuvius. Bull Volcanol 67:144–159

Gurioli L, Harris AJL, Houghton BF, Polacci M, Ripepe M (2008) Textural and geophysical characterization of explosive basaltic activity at Villarrica volcano. J Geophys Res 113. doi:10.1029/2007JB005328

Helz RT (1987) Diverse olivine types in lava of the 1959 eruption of Kilauea Volcano and their bearing on eruption dynamics. U S Geol Surv Prof Papers 1350:691–722

Holasek RE, Self S (1995) Goes weather-satellite observations and measurements of the May 18, 1980, Mount-St-Helens eruption. J Geophys Res-Solid Earth 100(B5):8469–8487

Houghton BF, Wilson CJN (1989) A vesicularity index for pyroclastic deposits. Bull Volcanol 51(6):451–462

Houghton BF, Wilson CJN, Del Carlo P, Coltelli M, Sable JE, Carey R (2004) The influence of conduit processes on changes in style of basaltic Plinian eruptions: Tarawera 1886 and Etna 122 BC. J Volcanol Geoth Res 137(1–3):1–14

Houghton BF, Carey RJ, Cashman KV, Wilson CJN, Hobden BJ, Hammer JE (2010) Diverse patterns of ascent, degassing, and eruption of rhyolite magma during the 1.8 ka Taupo eruption, New Zealand: evidence from clast vesicularity. J Volcanol Geoth Res 195(1):31–47

Klug C, Cashman KV (1994) Vesiculation of May 18, 1980, Mount St-Helens magma. Geol 22(5):468–472

Klug C, Cashman KV (1996) Permeability development in vesiculating magmas: implications for fragmentation. Bull Volcanol 58(2–3):87–100

Klug C, Cashman KV, Bacon CR (2002) Structure and physical characteristics of pumice from the climatic eruption of Mt Mazama (Crater Lake) Oregon. Bull Volcanol 64:486–501

Lara LE (2009) The 2008 eruption of the chaiten volcano, Chile: a preliminary report. Andean Geol 36(1):125–129

Lautze NC, Houghton BF (2005) Physical mingling of magma and complex eruption dynamics in the shallow conduit at Stromboli volcano, Italy. Geol 33:425–428

Lautze NC, Houghton BF (2007) Linking variable explosion style and magma textures during 2002 at Stromboli volcano, Italy. Bull Volcano 69:445–460

Lautze NC, Houghton BF (2008) Single explosions at Stromboli in 2002: use of clast microtextures to map physical diversity across a fragmentation zone. J Volcanol Geoth Res 170:262–268

Mangan MT, Cashman KV (1996) The structure of basaltic scoria and reticulite and inferences for vesiculation, foam formation, and fragmentation in lava fountains. J Volcanol Geoth Res 73(1–2):1–18

Mastin LG, Guffanti M, Servranckx R, Webley P, Barsotti S, Dean K, Durant A, Ewert JW, Neri A, Rose WI, Schneider D, Siebert L, Stunder B, Swanson G, Tupper A, Volentik A, Waythomas CF (2009) A multidisciplinary effort to assign realistic source parameters to models of volcanic ash-cloud transport and dispersion during eruptions. J Volcanol Geoth Res 186(1–2):10–21

Metrich N, Bertagnini A, Landi P, Rosi M (2001) Crystallization driven by decompression and water loss at Stromboli Volcano (Aeolian Islands, Italy). J Petrol 42:1471–1490

Parfitt EA (1998) A study of clast size distribution, ash deposition and fragmentation in a Hawaiian-style volcanic eruption. J Volcanol Geotherm Res 84:197–208

Parfitt EA, Wilson L (1999) A Plinian treatment of fallout from Hawaiian lava fountains. J Volcanol Geoth Res 88:67–75

Patrick, M (2005) Strombolian eruption dynamics from thermal (FLIR) video imagery, Ph.D. Thesis, University of Hawaii, Hawaii

Pistolesi M, Rosi M, Cioni R, Cashman KV, Rossotti A, Aguilera E (2011) Physical volcanology of the post-twelfth-century activity at Cotopaxi volcano, Ecuador: behavior of an andesitic central volcano. Geol Soc Am Bull 123(5–6):1193–1215

Rosi M, Landi P, Polacci M, Di Muro A, Zandomeneghi D (2004) Role of conduit shear on ascent of the crystal-rich magma feeding the 800-year-BP Plinian eruption of Quilotoa Volcano (Ecuador). Bull Volcanol 66(4):307–321

Rust AC, Cashman KV (2011) Permeability controls on expansion and size distributions of pyroclasts. J. Geophys. Res.-Solid Earth 116: B11202

Sable JE, Houghton BF, Del Carlo P, Coltelli M (2006) Changing conditions of magma ascent and fragmentation during the Etna 122 BC basaltic Plinian eruption: evidence from clasts micro-textures. J Volcanol Geoth Res 158:333–354

Sable JE, Houghton BF, Wilson CJN, Carey RJ (2009) Eruption mechanisms during the climax of the Tarawera 1886 basaltic Plinian eruption inferred from microtextural characteristics of the deposit. In: Self S, Larsen J, Rowland K, Hoskuldsson A, Thordarson T (eds) Studies in volcanology: the legacy of George Walker. Geol Soc, London

Sahagian DL, Proussevitch AA (1998) 3D particle size distribution from 2D observations: stereology for natural applications. J Volcanol Geoth Res 84:173–196

Shea T, Gurioli L, Larsen JF, Houghton BF, Hammer JE, Cashman KV (2010a) Linking experimental and natural vesicle textures in Vesuvius 79 AD white pumice. J Volcanol Geoth Res 192(1–2):69–84

Shea T, Houghton BF, Gurioli L, Cashman KV, Hammer JE, Hobden BJ (2010b) Textural studies of vesicles in volcanic rocks: an integrated methodology. J Volcanol Geoth Res 190(3–4):271–289

Shea T, Gurioli L, Houghton BF, Cioni R, Cashman KV (2011) Column collapse and generation of pyroclastic density currents during the AD 79 eruption of Vesuvius: the role of pyroclast density. Geol 39(7):695–698

Smithsonian Institution (2008) Chaitén. Bull Glob Volcan Netw, v. 33, no. 04-06

Sparks RSJ (1978) Dynamics of bubble formation and growth in magmas —review and analysis. J Volcanol Geoth Res 3(1–2):1–37

Stovall W, Houghton B, Gonnermann H, Fagents S, Swanson D (2011) Eruption dynamics of Hawaiian-style fountains: the case study of episode 1 of the Kīlauea Iki 1959 eruption. Bull Volcanol 73 (5):511–529

Sutton AN, Blake S, Wilson CJN (1995) An outline geochemistry of rhyolite eruptives from taupo volcanic center, New-Zealand. J Volcanol Geoth Res 68(1–3):153–175

Sutton AN, Blake S, Wilson CJN, Charlier BLA (2000) Late Quaternary evolution of a hyperactive rhyolite magmatic system: Taupo volcanic centre, New Zealand. J Geol Soc Lond 157:537–552

Tait S, Thomas R, Gardner J, Jaupart C (1998) Constraints on cooling rates and permeabilities of pumice in an explosive eruption jet from colour and magnetic mineralogy. J Volcanol Geoth Res 86 (1–4):79–91

Thomas RME, Sparks RSJ (1992) Cooling of tephra during fallout from eruption columns. Bull Volcanol 54(7):542–553

Toramaru A (1990) Measurement of bubble-size distributions in vesiculated rocks with implications for quantitative estimation of eruption processes. J Volcanol Geoth Res 43(1–4):71–90

Toramaru A (1995) Numerical study of nucleation and growth of bubbles in viscous magmas. J Geophys Res 100:1913–1931

Toramaru A (2006) BND (bubble number density) decompression rate meter for explosive volcanic eruptions. J Volcanol Geoth Res 154 (3–4):303–316

Verhoogen J (1951) Mechanics of ash formation. Am J Sci 249 (10):729–739

Walker GPL, Self S, Wilson L (1984) Tarawera, 1886, New Zealand—a basaltic Plinian fissure eruption. J Volcanol Geotherm Res 21:61–78

Wallace PJ, Anderson AT (1998) Effects of eruption and lava drainback on the H2O contents of basaltic magmas at Kilauea volcano. Bull Volcanol 59:327–344

Wicks C, de la Llera JC, Lara LE, Lowenstern J (2011) The role of dyking and fault control in the rapid onset of eruption at Chaiten volcano. Chile Nat 478(7369):374-+

Wilson CJN (1993) Stratigraphy, chronology, styles and dynamics of late quaternary eruptions from Taupo volcano, New-Zealand. Philos Trans R Soc Lond Ser a-Math Phys Eng Sci 343 (1668):205–306

Wilson CJN, Walker GPL (1985) The Taupo eruption, New-Zealand. 1. General-aspects. Philos Trans R Soc Lond Ser a-Math Phys Eng Sci 314(1529):199

Wilson L, Walker GPL (1987) Explosive volcanic-eruptions. 6. Ejecta dispersal in Plinian eruptions—the control of eruption conditions and atmospheric properties. Geophys J R Astron Soc 89(2):657–679

Witter JB, Kress VC, Delmelle P, Stix J (2004) Volatile degassing, petrology, and magma dynamics of the Villarrica lava lake, southern Chile. J Volcanol Geoth Res 134:303–337